Hindawi
International Journal of Aerospace Engineering
Volume 2022, Article ID 2828198, 12 pages
https://doi.org/10.1155/2022/2828198

Research Article

Optimization of UAV Airfoil Based on Improved Particle Swarm Optimization Algorithm

Tieying Jiang[1,2] **and Liang Jiang**[1,2]

[1]*Aerospace Times FeiHong Technology Company Limited, China Academy of Aerospace Electronics Technology, Beijing 100094, China*
[2]*Intelligent Unmanned System Overall Technology Research and Development Center, China Aerospace Science and Technology Group co., Ltd., Beijing 100094, China*

Correspondence should be addressed to Tieying Jiang; jtybest@163.com

Received 16 April 2022; Revised 8 June 2022; Accepted 24 June 2022; Published 12 July 2022

Academic Editor: Hao Chen

Airfoil optimization is an essential task in the aerodynamic layout design of the unmanned aerial vehicle (UAV). An objective optimization function was constructed based on the airfoil power factor and handling stability at various attack angles. The parametric mathematical model of the airfoil and aerodynamic parameter proxy model of airfoil were constructed using the Hicks-Henne improved function and CFD solution sample, focusing on the issues with particle swarm optimization algorithms such as slow convergence, a tendency to fall into local optimal solutions, and oscillation at a late stage; an optimization method for the low-speed airfoil of a small UAV based on improved particle swarm optimization was developed. When compared to standard particle swarm optimization, selective regenerative particle swarm optimization, and improved particle swarm optimization, the results indicate that the maximum thickness of the optimized rear airfoil decreases from 19.77% to 18.76%, the number of iterations decreases from 112 to 31, and the search speed of the improved particle swarm optimization significantly improves; the CFD results indicate that the optimized rear airfoil exhibits superior aerodynamic performance. On average, the airfoil's maximum lift-to-drag ratio is increased by 11.9%, its maximum power factor is increased by 12.5%, and its pitching moment is reduced by 8.4%. Within the UAV's speed range, the aerodynamic performance is stable.

1. Introduction

Airfoil is a critical component of the shape design of UAV wings, tail fins, and propellers [1]. The airfoil affects the cruise speed, takeoff and landing performance, stall speed, operational performance, and aerodynamic efficiency of the UAV throughout the flight cycle. It is a critical component of the aerodynamic and overall performance of the UAV [2]. The century-old development of airfoil research can be roughly divided into three stages [3–5]. The first stage from the beginning of the twentieth century to the 1950s, mainly in order to explore the mystery of more efficient flight of aircraft, carried out systematic research on airfoils and formed several general airfoil families. The second stage started from about the 1960s to the end of the twentieth century. With the continuous improvement of aircraft flight speed and the continuous improvement of performance index requirements, the need to develop more advanced airfoils became increasingly urgent. At the same time, the discovery of the supercritical airfoil principle has made the world's aviation powers begin to reemphasize airfoil research and has targeted the development of various modern airfoil families suitable for different types of aircraft and helicopters. The third stage is roughly from the beginning of the twenty-first century to the present. The rapid development of advanced numerical simulation methods, optimization design techniques, wind tunnel tests, and testing techniques has led to and promoted the research of various new airfoils. Under the constraints of complex engineering, an airfoil with excellent comprehensive performance is designed.

With the continuous expansion of the military use of UAVs, the tasks undertaken by UAVs have higher and

higher requirements for the basic performance of UAVs [6]. Selection and optimization of airfoils are critical tasks in UAV design [7, 8]. The conventional aerodynamic shape optimization of an airfoil is primarily investigated for large aircraft airfoils with Reynolds numbers in the order of magnitude of 10^7. Since the 1980s, high-altitude long-endurance UAVs have received extensive attention in military applications. In 1986, M.D. Maughmer and others designed the NASA NLF (1)-1015 airfoil for high-altitude long-endurance vehicles [9]. A low drag coefficient is achieved in long endurance states and in assault states. Since the design combines high lift coefficient and low Reynolds number, the velocity profile is designed with a "separation ramp" and a "curve transition ramp" to achieve higher lift and suppress the formation of laminar separation bubbles [10]. In the 1990s, NASA designed the LRN-1015 low Reynolds number airfoil for the wings of Northrop Grumman's RQ-4 "Global Hawk" high-altitude long-endurance UAV [11]. The flying height of the Global Hawk can reach 20 km, and the Reynolds number is only 500,000 under the condition of Mach 0.2. Under the design state, the laminar flow range on the upper and lower surfaces of the wing can reach 57% and 88% of the chord length, respectively, with low drag and higher lift-to-drag ratio. The excellent airfoil/wing aerodynamic performance and propulsion system make the "Global Hawk" UAV still the leader among the high-performance, high-altitude, and long-endurance large-scale military UAV platforms. In comparison, small UAVs are subject to low Reynolds numbers, typically in the orders of magnitude of $10^4 \sim 10^5$. When the Reynolds number is low, the flow around the airfoil is typically laminar, the flow momentum in the boundary layer is insufficient, and the adverse pressure gradient at the airfoil's tail easily causes airflow separation, which undoubtedly affects the airfoil's aerodynamic characteristics. Additionally, the purpose of optimizing a high Reynolds number airfoil is to obtain the optimal lift-drag ratio. While the purpose of optimizing a low Reynolds number airfoil is to improve the power factor, the UAV handling stability must also be considered.

In other countries, a parametric description based on standard airfoils was frequently used to improve the flight performance of small UAVs [12, 13]. Currently, the primary methods for airfoil parameterization are Hicks-Henne, Parsec Method, B-spline Curves, Mesh points, and CST [14–18], with the Hicks-Henne function and Parsec Method being the most frequently used. In recent years, evolutionary algorithms have been gradually introduced as optimization approaches, including iterative optimization of neural network prediction models and genetic algorithm optimization using Gaussian process regression [19, 20]. AtthaphonAriyarit used an evolutionary algorithm and a gradient-based method for multiobjective problems [21]. PhiboonTharathep proposed a multifidelity surrogate model and used nondominated sorting genetic algorithm II to solve multifidelity multiobjective airfoil design problem of UAV [22, 23]. An evolutionary algorithm is a type of heuristic search algorithm created by combining computer science and biology almost by corresponding laws [24]. Particle swarm optimization (PSO) is a significant subfield of evolutionary algorithms. It is an optimization algorithm based on a global random search strategy proposed in 1995 by Kennedy and Eberhart [25]. In 2006, Margarita Reyes Sierra carried out a summary study on the multiobjective optimization problem of particle swarm optimization algorithm [26]. Current PSO has been widely applied in various research fields, successfully resolving a wide variety of practical engineering problems, including task allocation and scheduling, data clustering, energy conservation in buildings, pattern recognition, shape design, and fault diagnosis [27–32]. Northwestern Polytechnical University used it in China to optimize the aerodynamic design of airfoil and wing [33]. PSO has some drawbacks when solving complex problems, including slow convergence, a proclivity to fall into local optimal solutions, and late-stage oscillation. Many attempts have been made to address these issues. Tsai and Kao proposed and demonstrated the efficiency and suitability of a selective regenerative PSO algorithm for multipeak optimization functions [34]. The method's feasibility in dealing with practical complex optimization problems was demonstrated by its application in data clustering [35].

The airfoil optimization objective function was established by considering the airfoil's power factor and handling stability; the Hicks-Henne function was parameterized for the airfoil. Tsai et al. then proposed an improved PSO algorithm based on selective regenerative PSO to address PSO's slow convergence, inclination to fall into local optimal solutions, and late-stage oscillation. The CFD solver was directly invoked to obtain aerodynamic parameters for the airfoil, and the optimal airfoil profile was finally obtained by iteratively solving the objective function for airfoil optimization. We analyzed the aerodynamic performance and robustness of the optimized airfoil.

2. Optimization Objective Function

In the range of low Reynolds number, the required power consumption P of small UAV in level flight can be simplified as

$$P = F_{\mathrm{T}}\mathrm{V}, \tag{1}$$

where $\mathrm{F_T}$ denotes propeller thrust and V denotes level flight speed.

According to the following formula:

$$F_T = \frac{mg}{K}, \tag{2}$$

$$0.5\rho V^2 S C_L = mg, \tag{3}$$

$$K = \frac{C_L}{C_D}. \tag{4}$$

The expression of required power consumption is

$$P = \mathrm{F_T V} = \frac{(\mathrm{mg})^{1.5}}{(0.5\rho S)^{0.5}} \frac{C_D}{C_L^{1.5}}, \tag{5}$$

where m denotes total flight mass of UAV; ρ denotes the density of incoming flow; S denotes wing area; K denotes the lift drag ratio of UAV; and C_L and C_D represent lift coefficient and drag coefficient. If the power factor is defined as $\mathrm{PI} = C_L^{1.5}/C_D$, greater PI leads to lower required power consumption P and is favorable to long endurance flight. The pitching moment coefficient C_{m} is a factor that must be considered in airfoil optimization design. In UAV flight, the excessively high absolute value C_{m} of airfoil will increase the trim drag and reduce the handling stability performance of the UAV. During the flight, the attack angle varies significantly with the change of combat mission, so it is required that C_{m} of airfoil should not be too large within a certain range of angle of attack. Otherwise, the handling stability performance of UAVs may be affected. Thus, the maximum power factor $PI_{\max}$ and the absolute value of the average pitching moment coefficient are the primary considerations in airfoil optimization. Since $PI_{\max_0}$ is usually hundreds of times of $|C_{\mathrm{m\_ave}_0}|$, the weight of $PI_{\max_0}$ and $|C_{\mathrm{m\_ave}_0}|$ is adjusted, and the optimization of the two objective functions is transformed into a single objective function problem [36, 37]. Therefore, the optimization objective function is set as follows:

$$\min\left(f\left(PI_{\max}, C_{m\_ave}\right)\right) = -k \times \mathrm{a}^{\left(\left|C_{m\_ave_0}\right| - \left|C_{m\_ave}\right|\right)^{1/b}} - a^{\left(PI_{\max} - PI_{\max_0}\right)^{1/c}}, \tag{6}$$

where k, a, b, and c are weight adjustment coefficients. $k \times \mathrm{a}^{\left(\left|C_{m\_ave_0}\right| - \left|C_{m\_ave}\right|\right)^{1/b}}$ and $a^{\left(PI_{\max} - PI_{\max_0}\right)^{1/c}}$ are the relevant terms of pitching moment coefficient and power factor of the objective function, respectively. Through the adjustment of the weight coefficient, the response of the power factor term and the pitch moment factor term of the objective function to $PI_{\max_0}$ and $C_{\mathrm{m\_ave}}$ is between [0,5], the response range tends to be consistent, and the response range of the objective function is between [−10, −1], as shown in Figures 1–3.

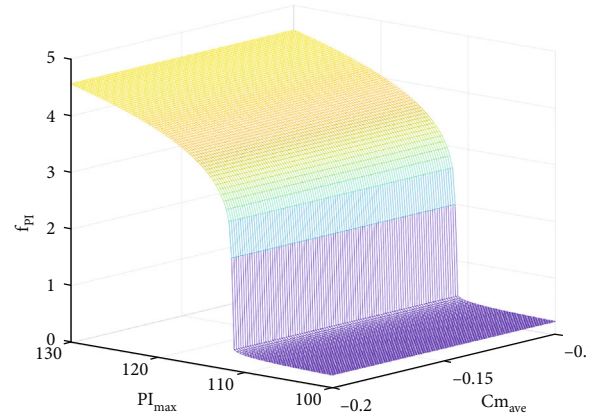

Figure 1: Power factor term.

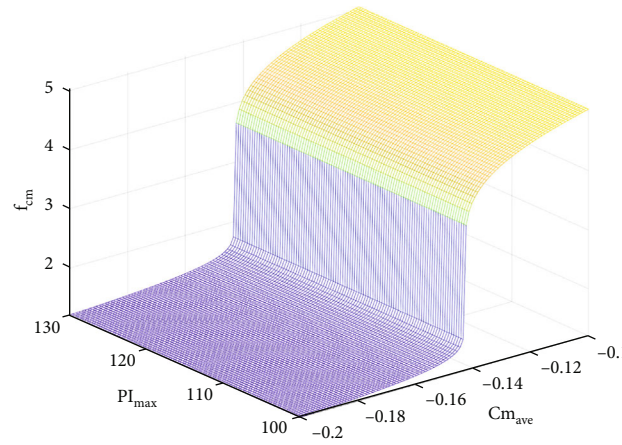

Figure 2: Pitching moment term.

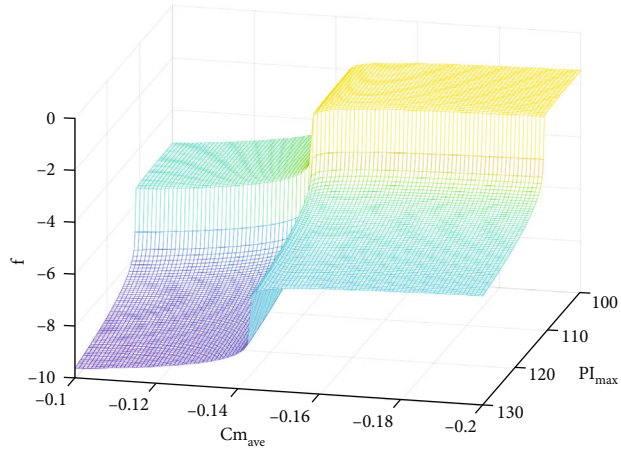

Figure 3: Objective function.

3. Algorithm

3.1. Particle Swarm Optimization. Each alternative PSO solution is transformed into a particle. Multiple particles coexist and search for optimization cooperatively. The optimal solution is determined iteratively using a randomly generated initial population, as illustrated in Figure 4. Each particle represents a candidate solution in the solution space, and the fitness function, which is defined according to the optimization criterion, determines the quality of the solution. As described below, particle velocities and positions are constantly updated to find the optimal solution.

(1) Initialization: Let the algorithm's search space be $\mathrm{D_S}$ dimensions and the total number of search particles be n_{pso}. The information of the i th particle can be expressed as

$$\mathbf{x}_{\mathrm{id}} = \left(x_{\mathrm{i1}}, x_{\mathrm{i2}}, \cdots, x_{\mathrm{iD_S}}\right), \tag{7}$$

where n_{pso} is population size. When the population size is too large, the algorithm's computing speed and convergence will be affected. But too small population size may affect the optimization efficiency of PSO. The initial particle population will be randomly generated within the

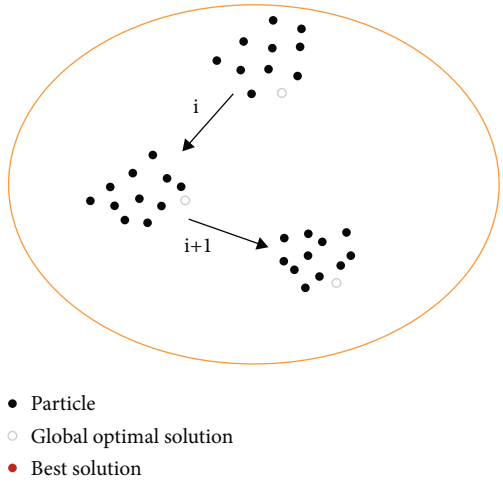

Figure 4: Particles finding the optimal solution with global best particle.

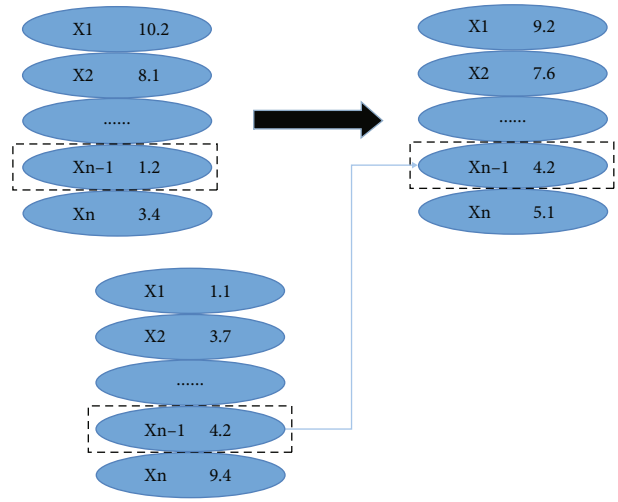

Figure 5: Particle regeneration.

motion range of the set parameters, and the position matrix $\mathbf{x}_{id}$ and velocity matrix $\mathbf{V}_{id}$ of the initial population will be formed.

(2) Update of velocity and position: each particle will seek a more advantageous position in space based on its own experience and that of neighboring particle swarms. The particle velocity and position are updated in accordance with the following:

$$\mathbf{V}_{id}^{new} = \omega \times \mathbf{V}_{id}^{old} + c_1 \times \xi \times \left(\mathbf{p}_{id}\text{-}\mathbf{x}_{id}^{old}\right) + c_2 \times \xi \times \left(\mathbf{p}_{gd}\text{-}\mathbf{x}_{id}^{old}\right), \tag{8}$$

$$\mathbf{x}_{id}^{new} = \mathbf{x}_{id}^{old} + \mathbf{V}_{id}^{new}, \tag{9}$$

where $\omega = 0.5 + (\xi/2)$ is inertia weight; ξ is a random number in 0 ~ 1; and c_1 and c_2 are the particle's local learning factor and global learning factor. By adjusting the size of the learning factor, the weights associated with self-summarizing and learning from excellent individuals in the particle's search process can be adjusted, bringing a single particle swarm closer to the optimal position in the swarm's history. p_{id} is the individual optimal particle position, which is the optimal location currently searched for the particle. p_{gd} is the global optimal particle position, which is the optimal position searched by the whole particle swarm so far; V_{id}^{old} and x_{id}^{old} are current velocity and position of the particle; $\mathbf{V}_{id}^{new}$ and $\mathbf{x}_{id}^{new}$ are updated speed and location of the particle.

(3) The individually optimal particle p_{id} and the globally optimal particle p_{gd} are selected by comparing the fitness values of particles

(4) Check of termination condition. Due to the iterative nature of PSO, the first termination condition is that the fitness of the optimal solution found by the algorithm is less than the minimum fitness threshold; the second termination condition is that the algorithm runs for the specified number of iterations. If the termination condition is satisfied, the iteration ends; otherwise, continue to Step (2)

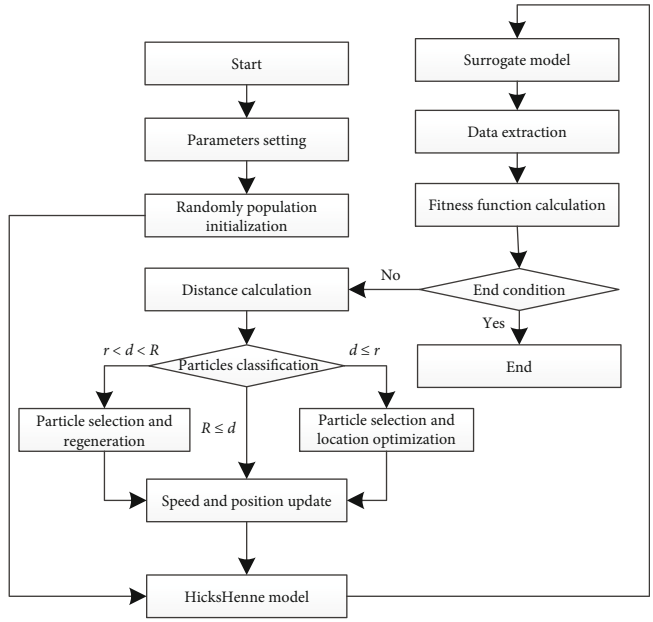

Figure 6: Flow chart of airfoil optimization algorithm.

3.2. Selective Regenerative PSO. Tsai found that particles close to p_{gd} did not contribute much to the search for the global optimal solution in the iterative process, so some particles with a distance d from p_{gd} that is less than R were selected to regenerate to find new areas. As a result, the likelihood of finding the global optimal solution was increased. The particles with the global optimal solution would not be selected during the selection process, allowing the search to continue in the current optimal direction. To retain the global optimal solution's position

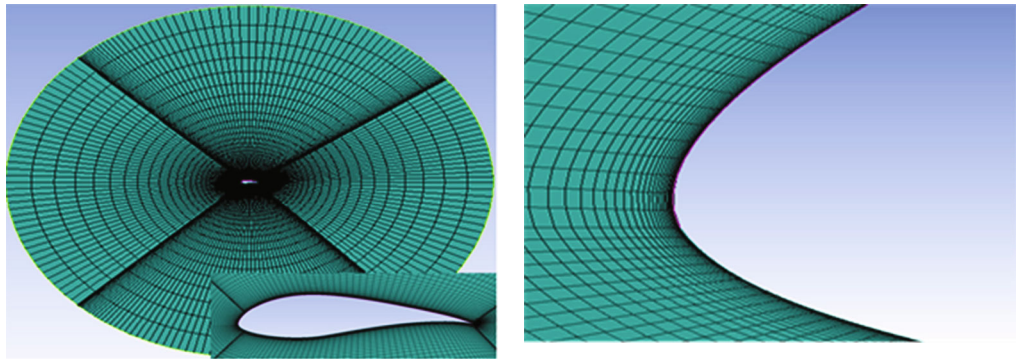

(a) Global grid computing (b) Near wall mesh

Figure 7: Schematic diagram of computational grid.

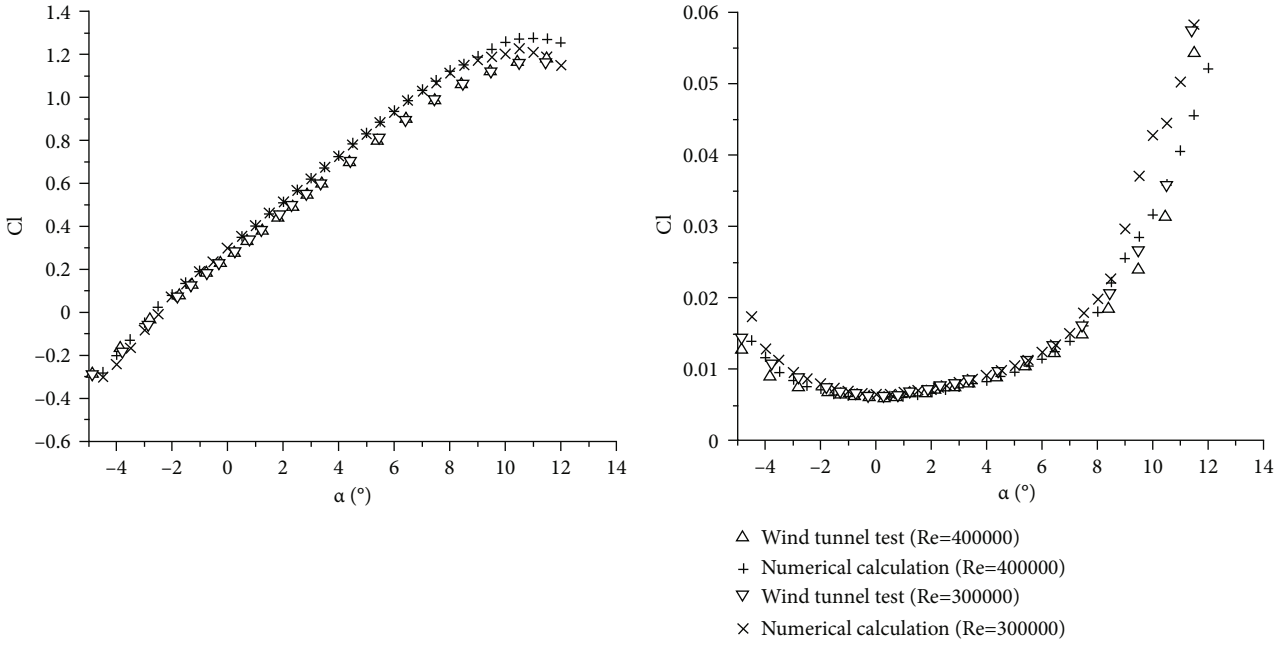

(a) Lift coefficient (b) Resistance coefficient

Figure 8: Numerical comparison of different Reynolds numbers for airfoil.

Table 1: Absolute and relative errors of RBF.

Type	PI_{max}		C_{m_ave}	
	Absolute error	Relative error	Absolute error of	Relative error
Average value	0.0018	0.0012	0.0009	0.0004

information, the position information of regenerative particles in each dimension has a certain probability of being assigned as the global optimal particle's position by a. Other positions have the probability of $(1\text{-}a)$ being randomly generated within the specified solution range, as shown in Figure 5. The selected regenerative particle's movement speed is specified in Equation (10) to avoid the selected regenerative particle from approaching the current global optimal particle.

Table 2: Optimization algorithm settings.

Parameters	Value	Parameters	Value
R	10^{-5}	c_2	2.5
r	0.5×10^{-5}	$\boldsymbol{f}_R$	0.4
$\bar{\omega}$	0.6	$\boldsymbol{f}_r$	0.8
E.G.	10^{-6}	$\boldsymbol{a}$	0.8
c_1	0.5	N_{iterm}	200

$$\boldsymbol{V}_{id}^{new} = \omega \times \boldsymbol{V}_{id}^{old} + c_2 \times \xi \times \left(\boldsymbol{p}_{id} - \boldsymbol{x}_{id}^{old}\right) + c_1 \times \xi \times \left(\boldsymbol{p}_{gd} - \boldsymbol{x}_{id}^{old}\right). \tag{10}$$

The selective regenerative PSO algorithm can regenerate particles close to the global optimal particle while

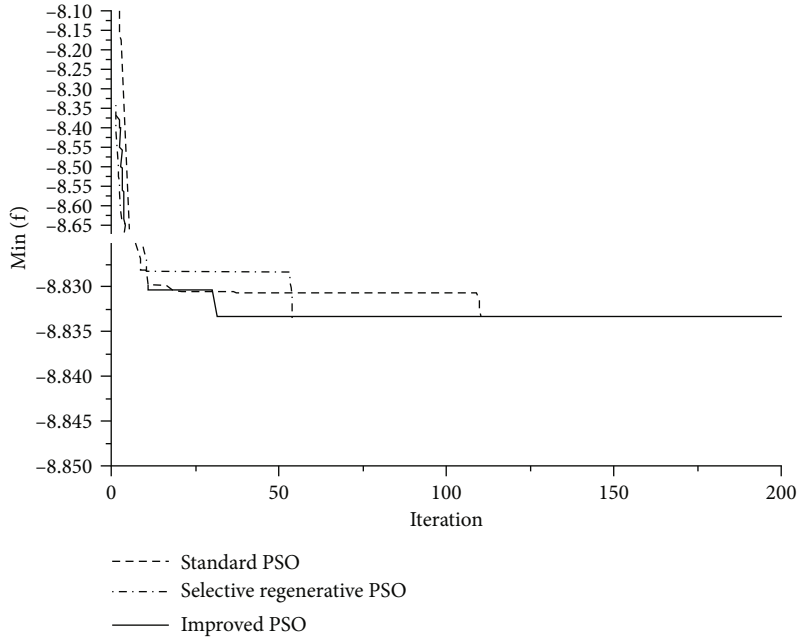

Figure 9: Iterative convergence curve.

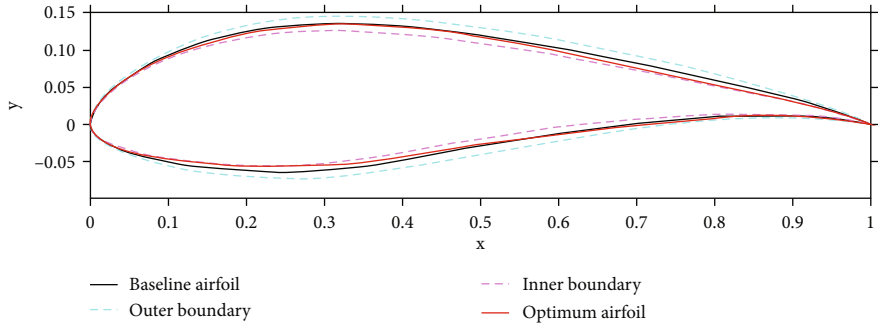

Figure 10: Comparison of airfoil profile before and after optimization.

reducing the ability of particles to optimize locally. As a result, this paper proposes an improved PSO.

3.3. Improved Particle Swarm Optimization. The improved PSO introduces some particles which are very close to the global best particle $\boldsymbol{p}_{\mathrm{gd}}$ for location optimization. It is not desirable, however, to have the direction of the newly located optimal particles pointed in the direction of the global best particle. Therefore, the local optimal particles' speeds are updated via Equation (10). The detailed procedure is described as follows:

(1) Distance calculation. Firstly, the distance d of each particle to the global best particle is calculated, as given by Equation (4). According to the distance, particles can be divided into three categories: $\mathrm{d} \geq R$, $\mathrm{r} < \mathrm{d} < \mathrm{R}$, and $\mathrm{d} \leq r$. R and r are predetermined values

$$d = \sum_{i=1}^{D_{\mathrm{S}}} \sqrt{\left(\mathrm{x}_i - \mathrm{x}_{\mathrm{gd}i}\right)^2}, \tag{11}$$

where d is the distance between the particle and P_{gd}; D_s is the dimensions of the particles and the number of the parameters to be identified; and x_i and x_{gdi} are the values of the ith dimension for the particle and $\boldsymbol{p}_{\mathrm{gd}}$.

(2) Particle selection and regeneration. Select a certain fraction f_R of these particles whose distance to the global best particle is $r < d < R$. These selected particles will regenerate, update velocity, and randomly generate individual best positions

(3) Particle selection and location optimization. For the particles whose distance to the global best particle is not greater than r, a certain fraction f_r of them are randomly selected for location optimization. In order to enhance the selected particles' local optimal ability, the selected particles' speeds are reduced:

$$\begin{cases} V_{\max\, r} = \varpi * V_{\max} \\ V_{\min\, r} = \varpi * V_{\min} \end{cases}, \tag{12}$$

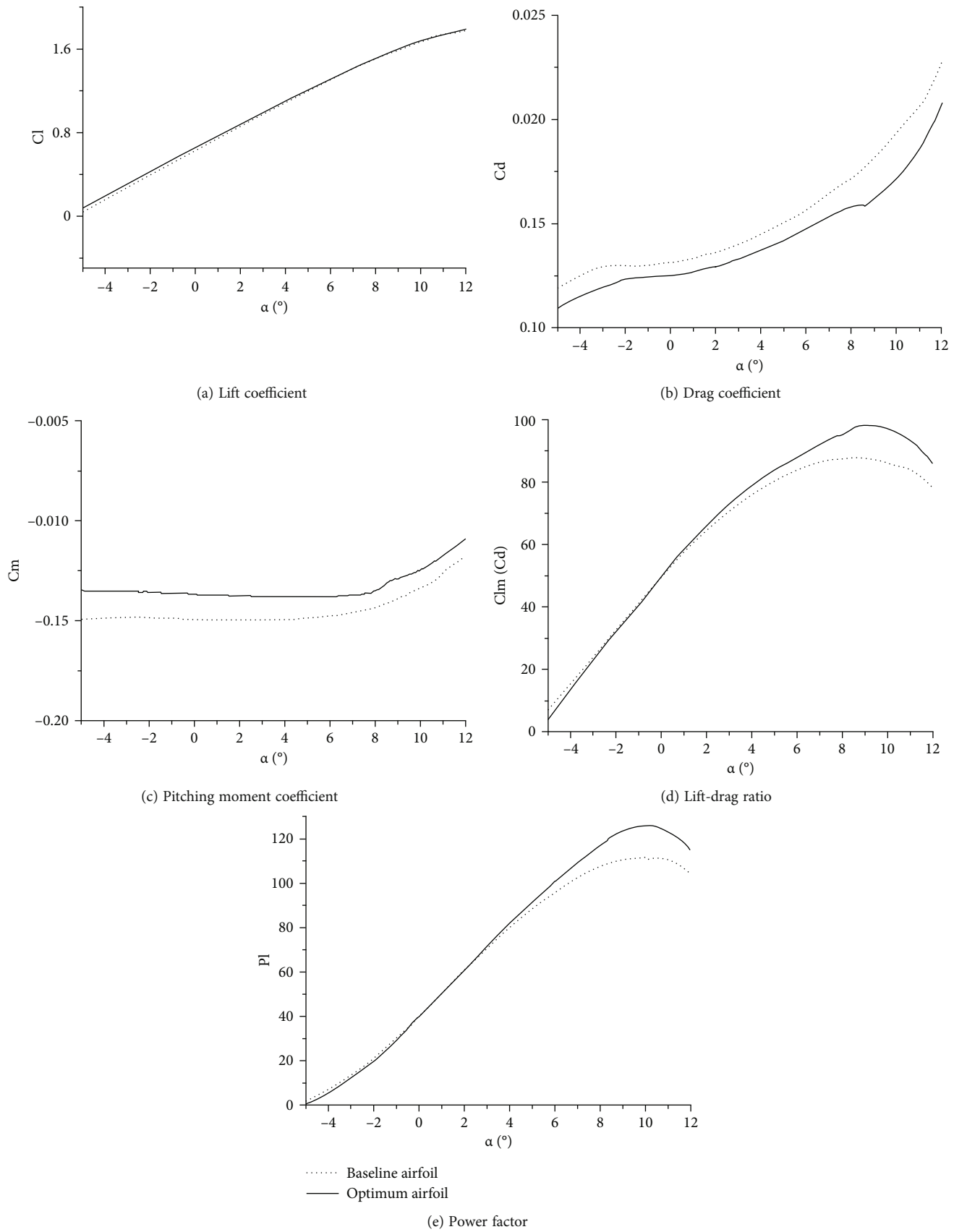

(a) Lift coefficient

(b) Drag coefficient

(c) Pitching moment coefficient

(d) Lift-drag ratio

(e) Power factor

Figure 11: Aerodynamic characteristics of airfoil with angle of attack.

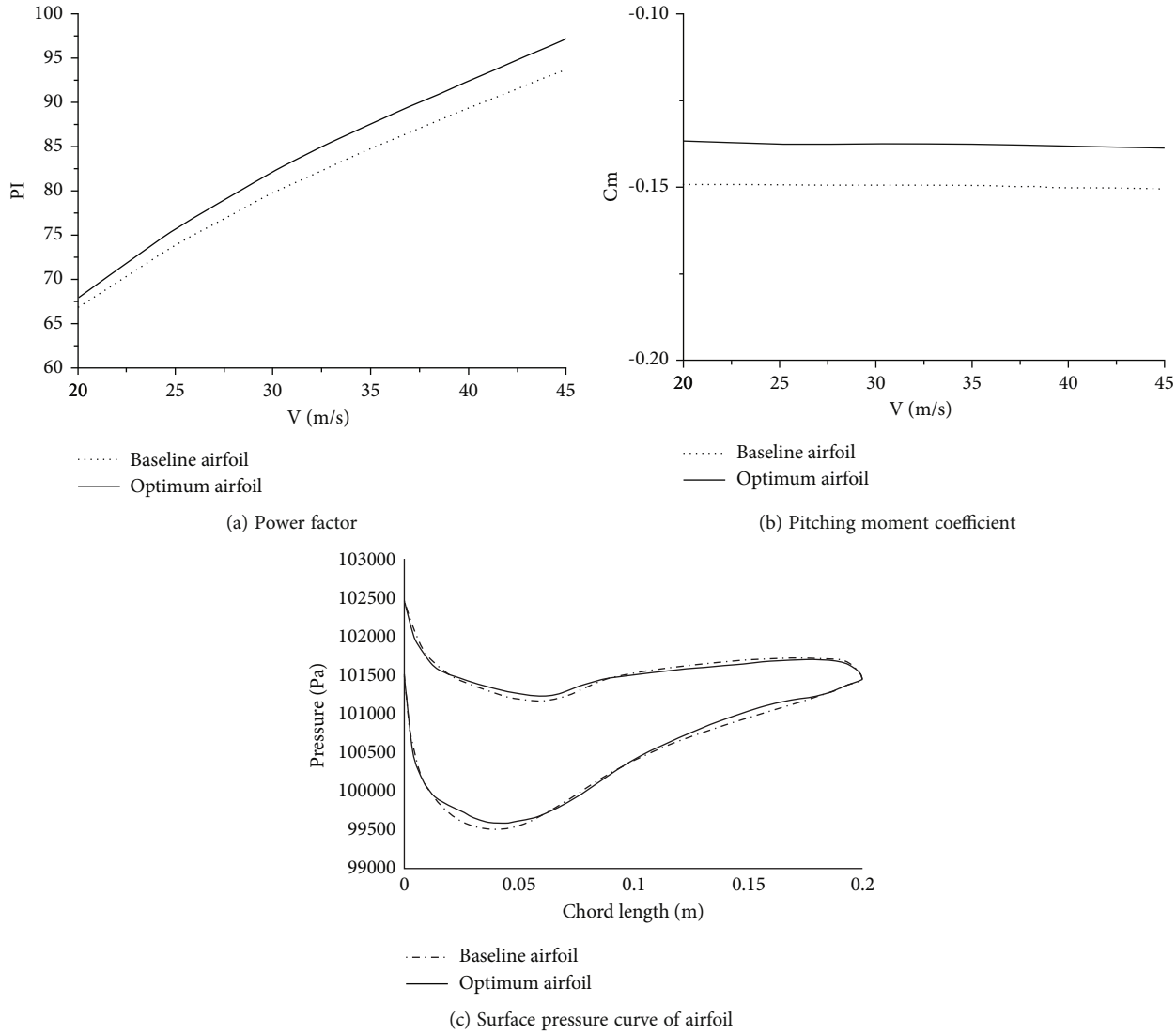

(a) Power factor

(b) Pitching moment coefficient

(c) Surface pressure curve of airfoil

Figure 12: Aerodynamic characteristics of airfoil with velocity.

where $V_{\max r}$ and $V_{\min r}$ are, respectively, the maximum and minimum speeds of the selected particles; ϖ is a scale factor in the range of (0,1); and $V_{\max}$ and $V_{\min}$ are the maximum and minimum speeds of the other particles, respectively. If Equation (8) is applied to update the selected particles' velocities, the search efficiency will be reduced, so the velocities and positions are updated according to Equations (9) and (10).

4. Optimization Design

4.1. Optimization Process. First, a favorable initial airfoil was chosen to obtain a good model coefficient through the fitting, and then the coefficient's variable range was determined. The improved PSO was then used to optimize the model coefficient. Following that, the surrogate model was directly invoked to obtain samples for analyzing aerodynamic characteristics, as illustrated in Figure 6.

4.2. Method of Airfoil Profile Parameterization. Hicks and Henne proposed the Hicks-Henne method for parameterized airfoil description [14]. The parameterization method is used to describe the change superimposed on the y-direction of a standard airfoil. Then, superimposition is used to reconstruct the airfoil profile using the coordinates of the basic airfoil. Assume that the coordinates of the upper and lower airfoil surfaces in the y-direction of the basic airfoil are $y_{0\mathrm{up}}(x)$ and $y_{0\mathrm{low}}(x)$ and that of the new airfoil are $y_{\mathrm{up}}(x)$ and $y_{\mathrm{low}}(x)$, respectively, then

$$y_{\mathrm{up}}(x) = y_{0\mathrm{up}}(x) + \sum_{k=1}^{k=n} \xi_k f_k(x),$$
$$y_{\mathrm{low}}(x) = y_{0\mathrm{low}}(x) - \sum_{k=1}^{k=n} \xi_{k+n} f_k(x), \tag{13}$$

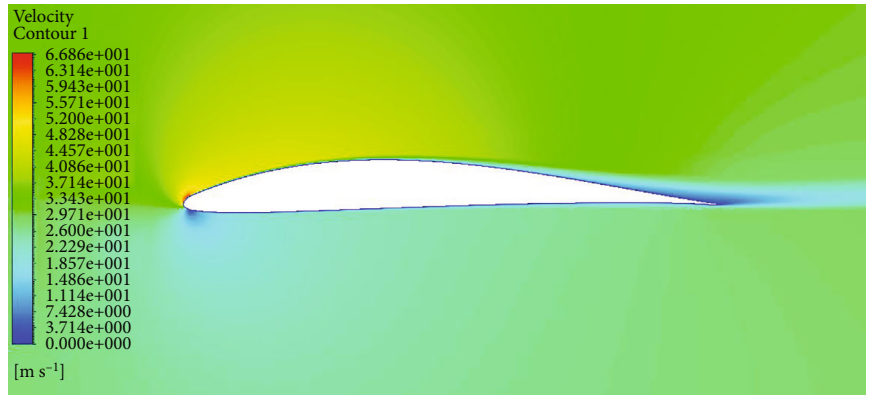

(a) Baseline airfoil

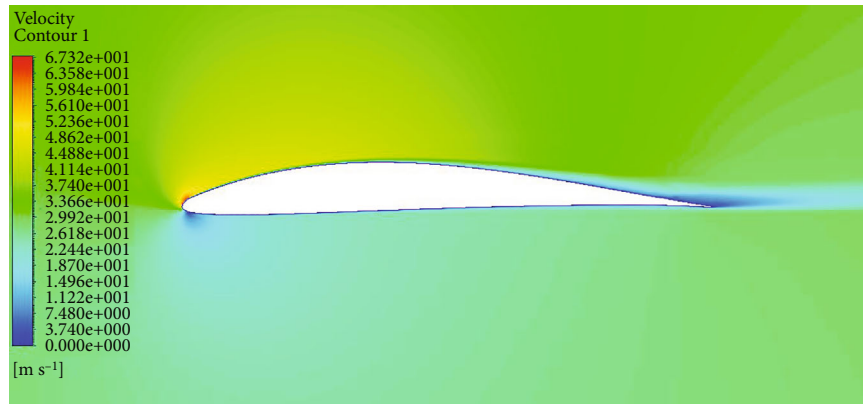

(b) Optimum airfoil

Figure 13: Comparison of flow field velocity cloud for baseline and optimum airfoils.

where ξ_k is the design variable of the new airfoil, usually on the order of 0.001; n is the number of type function; and $f_k(x)$ is a primary function. To reinforce the optimized airfoil's trailing edge optimization and to achieve control over the airfoil's trailing edge points, it is defined as

$$f_k(x) = \begin{cases} x^{0.25}(1-x)e^{-20x}, (k=1) \\ \sin^3\left(\pi x^{e(k)}\right), (2 \le k \le n-1), \\ ax(1-x)e^{-\beta(1-x)}, (k=n) \end{cases} \quad (14)$$
$$e(k) = \ln(0.5)/\ln x_k, (0 \le x_k \le 1).$$

The Hicks-Henne method suffers from a lack of trailing edge disturbance [38]. The airfoil profile's trailing edge disturbance function was optimized to provide effective trailing edge disturbance, as illustrated in the following equations:

$$f_n(x) = x(1-x)^{0.5}e^{-20(1-x)}, \quad (15)$$
$$f_n'(x) = \left(-20x^2 + 18x + 1\right)(1-x)^{0.5}e^{-20(1-x)}.$$

4.3. Flow Field Solving and Mesh Generation of the Airfoil. N-S equation was used as the main governing equation for flow field calculation [39], and space discretization was performed using the finite volume method. The field was solved on a density basis, and the flux difference was calculated using the Roe scheme. The Spalart-Allmaras (S-A) model was used as the turbulence model [40], and the spatial discretization scheme used was the upwind scheme with second-order accuracy. The pressure far field was chosen as the boundary condition, and the nonslip boundary was used for the airfoil wall. The airfoil calculation area was a circular area with the midpoint of the chord as the center and 20 times the length of the chord as the radius, and the grid distance near the wall was 1.0×10^{-6}, the number of grids was 21,000, and the structured O-shaped grid was generated as shown in Figure 7.

In order to ensure the reliability of the simulation results, the numerical calculation results were compared with the wind tunnel test results [41]. The results show that the numerical calculation results could accurately calculate the aerodynamic characteristics of the airfoil before the stall of the airfoil, as shown in Figure 8.

The radial basis function neural network (RBFNN) could be used to nonlinear fit the function. It had high prediction accuracy and strong generalization ability for individuals outside the learning samples. The input of the neural network were the parameterized parameters of the sample airfoil, and the corresponding maximum power factor, average coefficient of the pitching moment, and the output were the approximate mapping relationship between the

parameterized parameters and the maximum power factor, average coefficient of the pitching moment. In order to ensure the coverage of the training samples to the design space, this paper used the Latin hypercube method to generate 160 groups of initial training samples, 150 of which were used to train the neural network. The remaining 10 groups were used to test the prediction accuracy of the neural network. The average relative and absolute errors of the maximum power factor and the average coefficient of the pitching moment of the 10 groups of prediction samples are shown in Table 1. The relative error was the error of the predicted value of the proxy model for the lift resistance of the optimized airfoil relative to the CFD calculated value. The error accuracy had reached the order of 10^{-3}, which shows that the prediction accuracy of RBFNN is relatively high.

5. Result Analysis

In this paper, an airfoil is used as the reference airfoil for optimization, and the ambient states of airfoil analysis is as follows:

$$V = 30m/s, \mathrm{c} = 0.2m, \alpha = [-5, 12]^{\circ}. \tag{16}$$

The parameters of the improved PSO were configured as in Table 2, and the same were those of the standard PSO. The range of the parameters to be identified, $\xi_{\mathrm{i}}(i = 1, 2, \cdots \cdots, 12)$,was $[-0.005, 0.005]$.

The maximum number of optimization steps N_{iterm} was 200. To verify the convergence of the improved algorithm, the convergence criterion, E.G., was set to a minimum of 10^{-6}. Figure 9 depicts the objective function's iteration convergence curve. The improved PSO proposed in this paper iterates 31 times to find the optimal solution, whereas the selective regenerative PSO and the standard PSO iterate 52 and 112 steps, respectively, to find the optimal solution. The improved algorithm's optimization speed has increased significantly.

The comparison of the profiles before and after the dimensionless airfoil optimization is shown in Figure 10. The dashed lines represent the airfoil optimization's inner and outer boundary constraints, and the optimized airfoil's maximum thickness decreases from 19.77% to 18.76%. The comparison curves of aerodynamic characteristics before and after airfoil optimization are shown in Figure 11. As can be seen, the optimized rear airfoil's lift coefficient performance remains unchanged, but the drag coefficient and pitching moment both decrease significantly. The maximum lift-drag ratio $(C_l/C_d)_{\max}$ increases by 11.9%, the maximum power factor $\mathrm{PI}_{\max}$ increases by 12.5%, the average pitching moment $|C_{\mathrm{m\_ave}}|$ decreases by 8.4%, and the average drag $C_{\mathrm{d\_ave}}$ decreases by 6.7%.

To test the sensitivity of airfoil performance to incoming flow velocity, the aerodynamic characteristics of the airfoil in the range of 25 m/s~45 m/s were analyzed. Figures 12 and 13 are aerodynamic characteristic curves and velocity contours of the airfoil at different speeds with $\alpha = 4^{\circ}$. The flow separation phenomenon at the trailing edge of the optimized airfoil was lower than that of the basic airfoil, and the power factor of the optimized airfoil was better than that of the basic airfoil in the range of 25 m/s~45 m/s.

6. Conclusions

Airfoil is an important basic technology of aircraft. At present, with the increasing demand for small UAV flight capability, higher requirements are put forward for UAV airfoil, including higher power factor and better torque characteristics in mission state, which leads to the problem of airfoil optimization. To solve this problem, an optimization design method for the low-speed airfoil of small UAVs was proposed based on an improved PSO algorithm, The objective optimization function for the airfoil was established based on the power factor and handling of the airfoil. An improved PSO algorithm was proposed to address the PSO algorithm's slow convergence, inclination to fall into local optimal solutions, and late-stage oscillation. The results indicate that the improved PSO significantly improves search performance and reduces the number of iteration steps from 112 to 31; the aerodynamic performance of the optimized airfoil is improved considerably, the maximum power factor $\mathrm{PI}_{\max}$ increases by 12.5%, the average pitching moment $|C_{\mathrm{m\_ave}}|$ reduces by 8.4%, and the aerodynamic robustness and stability are strong. The future research work will further expand the optimization method, consider the Pareto solution problem in multi-objective optimization, and expand the application scope of the proposed method. In the aspect of optimization algorithm research, the results of more optimization methods are compared to continuously improve the identification performance of the model algorithm.

Data Availability

Some or all data, models, or code generated or used during the study are proprietary or confidential in nature and may only be provided with restrictions (e.g. anonymized data) and list items.

Conflicts of Interest

The authors declare that they have no conflicts of interest.

Acknowledgments

This project is supported by the Research and Development Fund of Chinese Equipment Development Department of the Central Military Commission, project number: 41411020301.

References

[1] H. A. Zhonghua, G. A. Zhenghong, S. O. Wenping, and X. I. Lu, "On airfoil research and development: history, current status, and future directions," *Acta Aerodynamica Sinica*, vol. 39, pp. 1–36, 2021.

[2] D. Raymer, *Aircraft Design: A Conceptual Approach*, AIAA, Inc., Washington, DC, 5th edition, 2012.

[3] J. D. Anderson, *Introduction to flight*, Mc Graw-Hill Book Company, Boston, 8th edition, 2008.

[4] G. D. Padfield and B. Lawrence, "The birth of flight control: an engineering analysis of the wright brothers' 1902 glider," *Aeronautical Journal*, vol. 2854, pp. 697–718, 2003.

[5] R. M. Hicks and P. A. Henne, "Wing design by numerical optimization," *Journal of Aircraft*, vol. 15, no. 7, pp. 407–412, 1978.

[6] T. Jiang, J. Yin, C. Yang, and J. Liang, "Identification method of SUAV in diving phase based on flight tests," *Mathematical Problems in Engineering*, vol. 2021, 13 pages, 2021.

[7] Z. Wei, Z. Ke, X. Lu, and Z. Gao, "A multi-disciplinary global/local optimization method for flying-wing airfoils design," *Acta Aerodynamica Sinica*, vol. 39, no. 6, pp. 37–52, 2021.

[8] Z. Gao and C. Wang, "Aerodynamic shape design methods for aircraft: status and trends," *Acta Aerodynamica Sinica*, vol. 35, no. 4, pp. 516–528, 2017.

[9] M. D. Maughmer and D. M. Somers, "Design and experimental results for a high-altitude, long-endurance airfoil," *Journal of Aircraft*, vol. 26, no. 2, pp. 148–153, 1989.

[10] R. Eppler and D. M. Somers, *Airfoil Design for Reynolds Numbers between 50, 000 and 500, 000*, NASA, 1985.

[11] L. F. Banal and A. T. Ubando, "Lift enhancement of the LRN 1015 airfoil using a gurney flap: a computational fluid dynamics investigation," *Journal of Computational Innovations and Engineering Applications*, vol. 2, no. 1, pp. 18–26, 2017.

[12] T. S. Tao, *Design and Development of a High-Altitude, in-Flight-Deployable Micro-UAV*, The Pennsylvania State University, 2010.

[13] Z. Huan, Z. Gao, and L. Xia, "Efficient robust aerodynamic design optimization method for high-speed NLF airfoil," *Acta Aeronautica et Astronautica Sinica*, vol. 43, no. 1, p. 124894, 2022.

[14] H. J. Kim, D. Sasaki, S. Obayashi, and K. Nakahashi, "Aerodyanmic optimization of supersonic transport wing using unstructured adjoint method," *AIAA Journal*, vol. 39, no. 6, 2001.

[15] L. He, W. Q.. Qian, T. Liu, X. C. Zhang, and K. S. Dong, "Inverse design method of airfoil based on deep learning," *Journal of Aerospace Power*, vol. 35, no. 9, pp. 1909–1917, 2020.

[16] S. Jeong, M. Murayama, and K. Yamamoto, *Efficient optimization design method using kriging model*, AIAA Aerospace sciences meeting and exhibit, Reno, Nevada, 2004.

[17] B. M. Kulfan, *A universal parametric geometry representation method-CST*, 45th AIAA Aerospace Sciences Meeting and Exhibit, Reno Hilton, 2007.

[18] C. Linsen, Z. Qianying, and X. Guo, "Airfoil optimization design based on Gaussian process regression and genetic algorithm," *Journal of Aerospace Power*, vol. 36, no. 11, pp. 2306–2316, 2021.

[19] B. Nvzi, P. Yehui, F. Heying, and Y. Chenghao, "Aerodynamic characteristic analysis and optimization design of four-parameter variable camber airfoil," *Mechanical Science and Technology for Aerospace Engineering*.

[20] M. Sessarego, K. R. Dixon, D. E. Rival, and D. H. Wood, "A hybrid multi-objective evolutionary algorithm for wind-turbine blade optimization," *Engineering Optimization*, vol. 47, no. 8, pp. 1043–1062, 2015.

[21] A. Ariyarit, M. Kanazaki, and S. Bureerat, "An approach combining an efficient and global evolutionary algorithm with a gradient-based method for airfoil design problems," *Smart Science*, vol. 8, no. 1, pp. 14–23, 2020.

[22] T. Phiboon, K. Khankwa, N. Petcharat et al., "Experiment and computation multi-fidelity multi-objective airfoil design optimization of fixed-wing UAV," *Journal of Mechanical Science and Technology*, vol. 35, no. 9, pp. 4065–4072, 2021.

[23] A. Ariyarit and M. Kanazaki, "Multi-fidelity multi-objective efficient global optimization applied to airfoil design problems," *Applied Sciences*, vol. 7, no. 12, p. 1318, 2017.

[24] S. P. Ni, H. T. Qi, and H. F. Li, "Hybrid algorithm based on multiple population genetic and mind evolution," *Computer Engineering*, vol. 47, no. 12, pp. 62–70, 2021.

[25] J. Kennedy and R. C. Eberhart, "Particle swarm optimization in neural networks proceedings," in *IEEE international conference*, pp. 1942–1948, New Jersey, USA, 1995.

[26] M. Reyes-Sierra and C. A. Coello Coello, "Multi-objective particle swarm optimizers: a survey of the state-of-the-art," *International Journal of Computational Intelligence Research*, vol. 2, no. 3, pp. 287–308, 2006.

[27] H. S. Wang, Z. H. Che, and C. Wu, "Using analytic hierarchy process and particle swarm optimization algorithm for evaluating product plans," *Expert Systems with Applications*, vol. 37, no. 2, pp. 1023–1034, 2010.

[28] L. Bo, L. Wang, and J. Yihui, "An effective hybrid PSO-based algorithm for low shop scheduling with limited buffers," *Computers and Operrations Research*, vol. 35, pp. 2791–2806, 2008.

[29] Y. T. Kao, E. Zahara, and I. W. Kao, "A hybridized approach to data clustering," *Expert Systems with Application*, vol. 34, no. 3, pp. 1754–1762, 2008.

[30] C.-J. Lin, J.-G. Wang, and C.-Y. Lee, "Pattern recognition using neural-fuzzy networks based on improved particle swam optimization," *Expert Systems with Application*, vol. 36, no. 3, pp. 5402–5410, 2009.

[31] P. Acharjee and S. K. Goswami, "Expert algorithm based on adaptive particle swarm optimization for power flow analysis," *Expert Systems with Applications*, vol. 36, no. 3, pp. 5151–5156, 2009.

[32] T. Jiang, J. Li, and K. Huang, "Longitudinal parameter identification of a small unmanned aerial vehicle based on modified particle swarm optimization," *Chinese Journal of Aeronautics*, vol. 28, no. 3, pp. 865–873, 2015.

[33] M. Chang, Y. Sun, J. Q. Bai, and X. X. Meng, "Aerodynamic design optimization of twice folding wing for tube-launched UAV constrained by flat-angle rotation mechanism," *Acta Aeronautica et Astronautica Sinica*, vol. 43, no. 9, p. 126339, 2022.

[34] C. Y. Tsai and I.-W. Kao, "A particle swarm with selective particle regeneration for multimodal functions," *WSEAS Transactions on Information Science and Applications*, vol. 6, no. 2, pp. 242–252, 2009.

[35] C.-Y. Tsai and I.-W. Kao, "Particle swarm optimization with selective particle regeneration for data clustering," *Expert Systems with Applications*, vol. 38, no. 6, pp. 6565–6576, 2011.

[36] R. T. Marler and J. S. Arora, "The weighted sum method for multi-objective optimization: new insights," *Structural and Multidisciplinary Optimization*, vol. 41, no. 6, pp. 853–862, 2010.

[37] S. Hemamalini and S. P. Simon, "Economic/emission load dispatch using artificial bee colony algorithm," *ACEEE International Journal on Electrical and Power Engineering*, vol. 1, pp. 212–217, 2010.

[38] W. Zhang, Q. Wang, J. Lu, and C. Yan, "Robust optimization design under geometric uncertainty based on PCA-Hicks Henne method," *Journal of Beijing University of Aeronautics and Astronautics*, 2021.

[39] J. D. Anderson, *Computational Fluid Dynamics the Basics With Applications*, Tsinghua University Press, Beijing, 2002.

[40] P. Spalart and S. Allmaras, "A one-equation turbulence model for aerodynamic flows," *La Recherche Aerospatiale*, vol. 1, no. 1, pp. 5–21, 1994.

[41] S. S. Michael and B. D. Granahan, "Wind tunnel testing airfoils at low Reynolds numbers," in *49th AIAA Aerospace Sciences Meeting Including the New Horizons Forum and Aerospace Exposition*, pp. 986–1000, Orlando, Florida, 2011.